Journal of Advanced Ceramics
2021, **10**(6): 1282–1290
https://doi.org/10.1007/s40145-021-0503-0

ISSN 2226-4108
CN 10-1154/TQ

Research Article

Sintering behaviour and microwave dielectric properties of $MgO–2B_2O_3–xwt\%BaCu(B_2O_5)–ywt\%H_3BO_3$ ceramics

Haiquan WANG, Shixuan LI, Kangguo WANG, Xiuli CHEN, Huanfu ZHOU*

Collaborative Innovation Center for Exploration of Hidden Nonferrous Metal Deposits and Development of New Materials in Guangxi, Key Laboratory of Nonferrous Materials and New Processing Technology, Ministry of Education, School of Materials Science and Engineering, Guilin University of Technology, Guilin 541004, China

Received: March 21, 2021; Revised: May 20, 2021; Accepted: May 27, 2021

Abstract: This study investigates the bulk density, sintering behaviour, and microwave dielectric properties of the $MgO–2B_2O_3$ series ceramics synthesised by solid-state reaction. According to the X-ray diffraction and microstructural analyses, the as-prepared $MgO–2B_2O_3$ ceramics possess a single-phase structure with a rod-like morphology. The effects of different quantities of H_3BO_3 and $BaCu(B_2O_5)$ (BCB) on the bulk density, sintering behaviour, and microwave dielectric properties of the $MgO–2B_2O_3$ ceramics were investigated. Accordingly, the optimal sintering temperature was obtained by adding 30 wt% H_3BO_3 and 8 wt% BCB. We also reduced the sintering temperature to 825 ℃. Furthermore, the addition of 40 wt% H_3BO_3 and 4 wt% BCB increased the quality factor, permittivity, and temperature coefficient of resonance frequency of $MgO–2B_2O_3$ to 44,306 GHz (at 15 GHz), 5.1, and −32 ppm/℃, respectively. These properties make $MgO–2B_2O_3$ a viable low-temperature co-fired ceramic with broad applications in microwave dielectrics.

Keywords: low-temperature co-fired ceramics (LTCC); sintering temperature; $MgO–2B_2O_3$; H_3BO_3; microwave dielectrics; temperature coefficient of resonance frequency

1 Introduction

Low-temperature co-fired ceramics (LTCC) are widely used in the wireless communication and broadcasting industries as raw materials for manufacturing electronic components, owing to their low manufacturing cost, short development cycle, and potential for the miniaturisation of electronic devices [1–4]. However, most high $Q \times f$ dielectric materials are manufactured at high sintering temperatures, which hinder their incorporation with low melting-point electrodes and polymer-based substrates and lead to excess energy consumption and evaporation of volatile components. For practical application, LTCC requires excellent microwave dielectric properties, low sintering temperature, and adequate co-fire matching between ceramics and electrodes [5–10]. Materials with low melting points are often added to LTCC to reduce the required firing temperatures. However, this approach weakens the microwave dielectric properties.

$MgO–B_2O_3$ ceramics have drawn research interest because of its potential applications in LTCC devices. Davis and Knight [11] systematically reported the chemistry of $MgO–B_2O_3$ binary systems, i.e., $MgO–B_2O_3$, $MgO–1/2B_2O_3$, and $MgO–1/3B_2O_3$. Nishizuka *et al*. [12] demonstrated that the $MgO–xB_2O_3$ (x = 25 and 33)

* Corresponding author.
E-mail: zhouhuanfu@163.com

sintered at low temperatures exhibited remarkable dielectric properties with a permittivity (ε_r) of approximately 7 and quality factors ($Q \times f$) of 79,100–260,100 GHz (x = 33) and 39,600–310,000 GHz (x = 25). Peng *et al*, [13,14] reported the synthesis of $0.8Zn_3B_2O_6 + 0.2Mg_3B_2O_6$ composite ceramics for LTCC applications and obtained excellent dielectric properties at 950 ℃ sintering with a ε_r of 6.47, $Q \times f$ of 89,600 GHz, and temperature coefficient of resonance frequency (τ_f) of approximately 48.6 ppm/℃.

In addition, optimized $Zn_3B_2O_6$ ceramics using Ni^{2+} instead of Zn^{2+} were reported with strong dielectric properties at 900 ℃ with a ε_r of 6.9, $Q \times f$ of 91,000 GHz, and τ_f of approximately 55.6 ppm/℃. Peng *et al*. [15] reported $Li_2(Mg_{1-x}Ni_x)SiO_4$ ceramics with the addition of 2 wt% lithium–boron–bismuth–silicon (LBBS) glass and realised excellent dielectric properties at 900 ℃ (sintering) and microwave dielectric properties. Fan *et al.* [16] reported optimal microwave dielectric properties at a sintering temperature as low as 1100 ℃ with a molecular ratio of MgO : B_2O_3 = 1 : 1. The resulting ceramics demonstrated strong microwave dielectric properties with a ε_r of 5.83, $Q \times f$ of 41,930 GHz, and τ_f of approximately 62 ppm/℃. According to Zhou *et al.* [17], MgO–$2B_2O_3$–4wt%$BaCu(B_2O_5)$ ceramics possess appropriate microwave dielectric properties, showing promise in LTCC applications.

However, the microwave dielectric properties of B_2O_3-rich ceramics in a MgO–B_2O_3 binary system (e.g., MgO–$2B_2O_3$ and MgO–B_2O_3) have not been investigated in detail. In addition, the sintering temperature of MgO–$2B_2O_3$ ceramics remains considerably high for LTCC devices [18]. Sintering additives [19–29], ultrafine powders [30–34], and low-sintering-temperature materials [35–37] can be used to reduce the sintering temperature of ceramics. However, the preparation of ultrafine powder with low intrinsic sintering temperatures is expensive, complex, and difficult to expand for commercialisation. Glass exhibits much lower $Q \times f$ value than pure microwave dielectric ceramics [38]. Therefore, when microwave ceramics are doped with glass, the quality factor decreases [1,39]. $BaCu(B_2O_5)$ (BCB) has a low melting temperature, adequate wettability, and strong microwave dielectric properties. Therefore, its addition for sintering will contribute to the densification of $Mg_3B_2O_6$ ceramics [24,40]. Furthermore, researchers effectively reduced the sintering temperature of MgO by adding the appropriate amount of sintering materials [37], such as B_2O_3, H_3BO_3, and BCB. However, the microwave dielectric properties of MgO–$2B_2O_3$–$x$wt%BCB–$y$wt%H_3BO_3 ceramics have not been investigated systematically, which is the objective of this research.

2 Experimental

MgO–$2B_2O_3$–$x$wt%BCB–$y$wt%H_3BO_3 ceramics were prepared using solid-state reaction method. MgO (≥ 98.5%), H_3BO_3 (≥ 99%), $Ba(HO)_2 \cdot 8H_2O$ (≥ 99%), and CuO (≥ 99%) were acquired from Guo-Yao Co., Ltd., Shanghai, China. MgO powder was pre-calcined at 800 ℃ for 2 h. The raw materials were weighed according to the molar ratio of MgO : B_2O_3 = 1 : 2. The powders were mixed thoroughly in a nylon jar before ball milling for 4 h. Then, the dried powder mixture was calcined at 800 ℃ for 4 h. H_3BO_3 and BCB with different mass ratios were added to the calcined powder. The mixture of H_3BO_3, BCB, and calcined powder was re-milled for 4 h and pressed into the form of cylinder with a diameter of 10 mm and a height of 4–5 mm, under a uniaxial pressure of 100 MPa. Pellets were fired at 550 ℃ for 4 h to eliminate polyvinyl alcohol (PVA). Subsequently, the samples were sintered for 4 h at 750–975 ℃ in air.

Archimedes' principle was employed to measure the bulk density. X-ray diffractometer (X'PERT PRO, PANalytical, Almelo, the Netherlands), equipped with Cu Kα radiation instrument (λ = 0.15406 nm), was used for the structural analysis. Scanning electron microscope (SEM; JSM-6380LV, JEOL, Tokyo, Japan) was used to observe the microstructure of the as-fired surfaces. A 300 kHz–20 GHz network analyzer (E5071C, Agilent Co., CA, USA) was used to measure the microwave dielectric properties. The τ_f values were calculated in the temperature range of 25–85 ℃ using the following expression:

$$\tau_f = \frac{f_T - f_{T0}}{f_{T0}(T - T_0)} \times 10^6 \quad (1)$$

where f_T and f_{T0} represent the resonant frequencies at 85 ℃ (T) and 25 ℃ (T_0), respectively.

3 Results and discussion

Figure 1 illustrates the XRD profiles of MgO–$2B_2O_3$–$x$wt%BCB–10wt%H_3BO_3 (x = 2, 4, 6, and 8) ceramics sintered at their optimal temperatures. The XRD

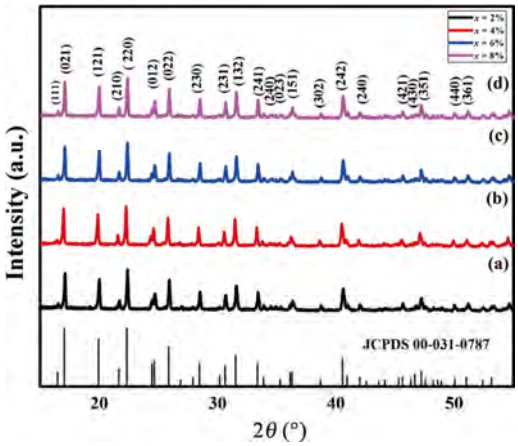

Fig. 1 XRD patterns of $MgO–2B_2O_3–x$wt%BCB–10wt%H_3BO_3 (x = 2, 4, 6, and 8) ceramics sintered at their optimal temperatures: (a) x = 2, 950 ℃, (b) x = 4, 925 ℃, (c) x = 6, 850 ℃, and (d) x = 8, 825 ℃.

patterns were indexed as MgB_4O_7 (JCPDS Card No. 00-031-0787), indicating that the addition of H_3BO_3 and BCB had no effect on the phase structure of the ceramics.

Figures 2(a)–2(d) illustrate the SEM images of the $MgO–2B_2O_3–x$wt%BCB–10wt%H_3BO_3 (x = 2, 4, 6, and 8) ceramics sintered at optimal temperatures. The $MgO–2B_2O_3$ crystals possess a rod-like shape and are refined with the increase in the BCB content. As the BCB content increased to 8 wt%, the $MgO–2B_2O_3$ crystals exhibited a glassy phase. Moreover, the porosity increased with the increase in BCB content. When x = 4, two grains of the $MgO–2B_2O_3–x$wt%BCB–10wt%H_3BO_3 ceramics with the optimal sintering temperature of 925 ℃ were selected for the energy dispersive X-ray spectroscopy (EDS) test. Table 1 lists the results of this test. The grains in region I consist of Mg, B, O, Cu, and Ba in the molar ratio of Mg : B : O = 29.78 : 17.14 : 52.28. Therefore, the compositions of the grains in regions I and II are $MgB_{0.58}O_{1.8}$ and MgB_4O_7, respectively.

Figure 3 depicts the bulk density, ε_r, $Q \times f$, and τ_f of the $MgO–2B_2O_3–x$wt%BCB–10wt%H_3BO_3 (x = 2, 4, 6, and 8) ceramics sintered at different temperatures. As the sintering temperature increased, the bulk density initially increased, indicating that the samples became denser, and then decreased slightly (Fig. 3(d)). Subsequently, the increase in porosity of the samples owing to the high sintering temperature decreased the bulk density. The bulk density change remains consistent with the appearance of porosity, as shown in Figs. 2(a)–2(d).

When sintering temperature was increased from 900 to 950 ℃, the $Q \times f$ of the $MgO–2B_2O_3–2$wt%BCB–10wt%H_3BO_3 ceramics increased from 25,408 to 33,951 GHz, highlighting a change in porosity with a change in the sintering temperature. The minimum porosity was obtained at 900 ℃. However, with the further increase in the sintering temperature, the $Q \times f$ of the $MgO–2B_2O_3–2$wt%BCB–10wt%H_3BO_3 ceramics decreased to 32,541 GHz due to over-firing. The $Q \times f$ of $MgO–2B_2O_3–x$wt%BCB–10wt%H_3BO_3 (x = 2, 4, 6, and 8) ceramics first increased and then decreased with the increase in sintering temperatures.

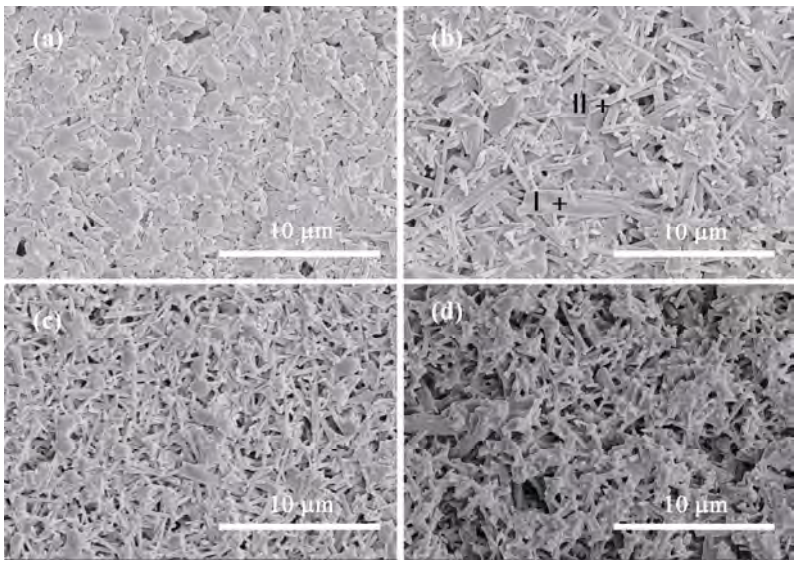

Fig. 2 SEM images of $MgO–2B_2O_3–x$wt%BCB–10wt%H_3BO_3 ceramics sintered at their optimal temperatures for 4 h: (a) x = 2, 950 ℃, (b) x = 4, 925 ℃, (c) x = 6, 850 ℃, and (d) x = 8, 825 ℃.

Table 1 EDS results of MgO–2B_2O_3–4wt%BCB–10wt%H_3BO_3 ceramics

Spot	Atom element (%)				
	Mg (K)	B (K)	O (K)	Cu (K)	Ba (K)
I	29.78	17.14	52.28	0.68	0.13
II	12.28	39.62	47.74	0.21	0.15

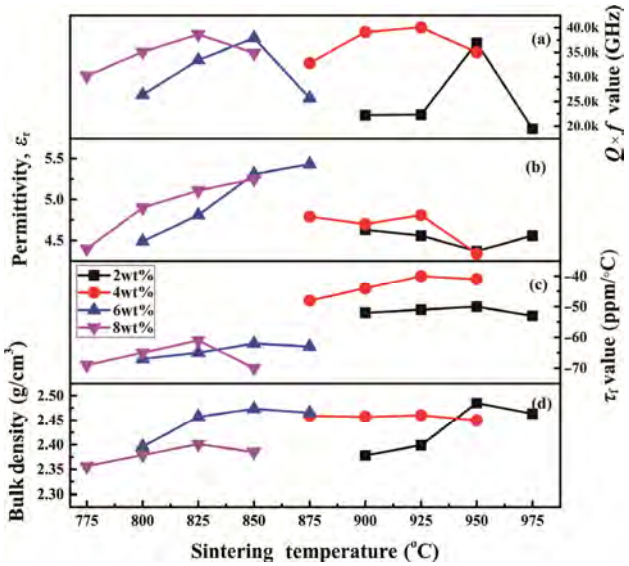

Fig. 3 Variation in bulk density, ε_r, $Q \times f$, and τ_f values of MgO–2B_2O_3–*x*wt%BCB–10wt%H_3BO_3 (*x* = 2, 4, 6, and 8) ceramics after sintering at different temperatures.

The optimal sintering temperature decreased from 950 to 850 ℃ when BCB content increased from 2 to 8 wt%. The $Q \times f$ reached a maximum of 40,076 GHz at 4 wt% BCB, indicating that the addition of the appropriate amount of BCB reduced the sintering temperature and improved the $Q \times f$ of the MgO–2B_2O_3–10wt%H_3BO_3 ceramics.

Figure 3(b) illustrates the change in ε_r of the MgO–2B_2O_3–*x*wt%BCB–10wt%H_3BO_3 (*x* = 2, 4, 6, and 8) ceramics at different temperatures. The ε_r of ceramics with 6 and 8 wt% BCB increased with the increase in the sintering temperature, whereas that of ceramics with 2 and 4 wt% BCB decreased, indicating that the addition of BCB had a significant effect on the ε_r of the MgO–2B_2O_3 ceramics.

Figure 3(c) presents τ_f at different sintering temperatures, which exhibits a trend similar to that of $Q \times f$. The τ_f of the MgO–2B_2O_3–2wt%BCB–10wt%H_3BO_3 ceramic was –40 ppm/℃ at a sintering temperature of 925 ℃. It initially increased with the increase in the sintering temperature and then decreased marginally. Therefore, τ_f is affected by the chemical additives and composition of the ceramic [37,41]. Notably, the τ_f of the MgO–2B_2O_3–*x*wt%BCB–10wt%H_3BO_3 ceramics demonstrated an overall decreasing trend with increasing BCB content. Additionally, the sintering temperature decreased with the increase in the BCB content, demonstrating its ability as a sintering aid. The optimal ceramic properties with a bulk density of 2.409 g/cm^3, $Q \times f$ of 40,076 GHz, and ε_r of –40 ppm/℃ were obtained at 4 wt% BCB and a sintering temperature of 925 ℃.

Figure 4 presents the room-temperature XRD profiles of the MgO–2B_2O_3–4wt%BCB–*y*wt%H_3BO_3 ($10 \leqslant y \leqslant 40$) ceramics sintered at their optimal temperatures. The results showed that the MgO–2B_2O_3–4wt%BCB–*y*wt%H_3BO_3 ($10 \leqslant y \leqslant 40$) ceramics were crystallised in the orthorhombic space group *Pbca* without impurity phases, indicating that the addition of H_3BO_3 had no negative effect on the phase structure of the ceramics.

Figure 5 presents the SEM images of the MgO–2B_2O_3–4wt%BCB–*y*wt%H_3BO_3 ($10 \leqslant y \leqslant 40$) ceramics sintered at their optimal temperatures. A distinct microstructure was observed for the ceramics with different H_3BO_3 contents. With the increase in the H_3BO_3 content, the MgO–2B_2O_3–4wt%BCB–*y*wt%H_3BO_3 ceramics achieved denser, more homogeneous microstructures. However, at 40 wt% H_3BO_3, a mild over-burning was observed owing to the presence of excessive sintering aid, resulting in an abnormal grain growth, as shown in Fig. 5(d). The EDS test of MgO–2B_2O_3–4wt%BCB–*y*wt%H_3BO_3 ceramic as *y* = 40 sintered at 900 ℃ was carried out to identify the

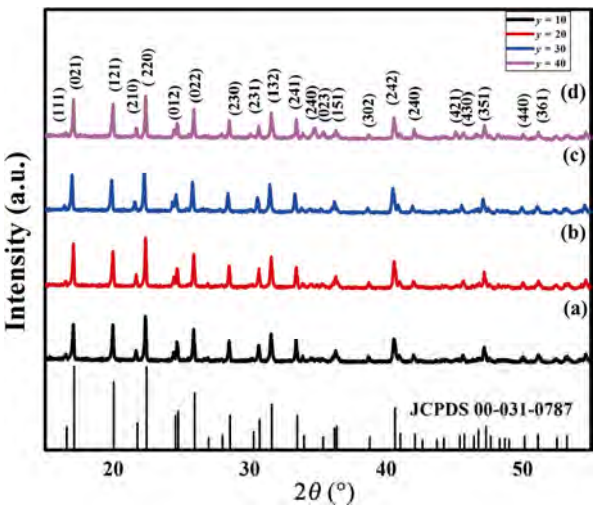

Fig. 4 XRD patterns of the MgO–2B_2O_3–4wt%BCB–*y*wt%H_3BO_3 ($10 \leqslant y \leqslant 40$) ceramics sintered at different temperature: (a) *y* = 10, 925 ℃, (b) *y* = 20, 900 ℃, (c) *y* = 30, 900 ℃, and (d) *y* = 40, 900 ℃.

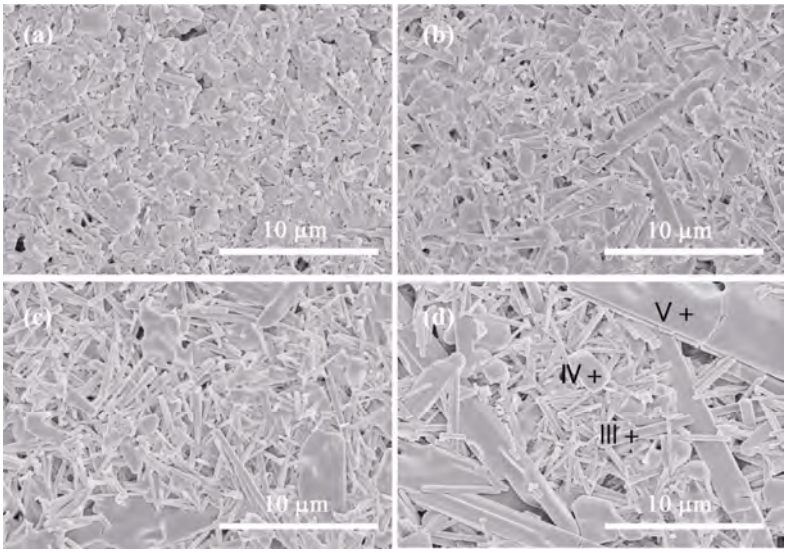

Fig. 5 SEM images of $MgO–2B_2O_3–4wt\%BCB–ywt\%H_3BO_3$ (y = 10, 20, 30, and 40) ceramics sintered at their optimal temperatures: (a) y = 10, 925 ℃, (b) y = 20, 900 ℃, (c) y = 30, 900 ℃, and (d) y = 40, 900 ℃.

composition, as shown in Table 2. Owing to the low instrumental precision, the Mg : B : O molar ratios of regions III, IV, and V were 10.85 : 41.05 : 47.75, 15.71 : 33.81 : 50.28, and 15.87 : 30.43 : 53.62, respectively. In addition, as the molar ratio of Cu and Ba in region III was approximately 1 : 1, the grain composition of this region contains MgB_4O_7 and BCB. The grains in regions IV and V can be considered as $MgB_{2.2}O_{3.2}$ and $MgB_{1.9}O_{3.2}$, respectively. This confirms the results of the MgB_4O_7 phase formation.

Figure 6 illustrates the bulk density, ε_r, $Q \times f$, and τ_f of the $MgO–2B_2O_3–4wt\%BCB–ywt\%H_3BO_3$ ceramics at different sintering temperatures. The bulk density of the ceramics initially increased and then slightly decreased with the increase in the H_3BO_3 content, except for those with 10 wt% H_3BO_3. The maximum bulk density of $MgO–2B_2O_3–4wt\%BCB–ywt\%H_3BO_3$ with 10 wt% H_3BO_3 was obtained at a sintering temperature of 925 ℃. However, when H_3BO_3 increased to 20–40 wt%, the maximum bulk density was obtained at 900 ℃, indicating that the addition of H_3BO_3 as a sintering aid reduced the sintering temperature of the ceramics.

Table 2 EDS results of $MgO–2B_2O_3–4wt\%BCB–40wt\%H_3BO_3$ ceramics

Spot	Atom element (%)				
	Mg (K)	B (K)	O (K)	Cu (K)	Ba (K)
III	10.85	41.05	47.75	0.16	0.18
IV	15.71	33.81	50.28	0.19	0.01
V	15.87	30.43	53.62	0.07	0.02

In general, the $Q \times f$ of microwave dielectric ceramics is related to the grain size, porosity, densification, and secondary phases [42–44]. The $Q \times f$ of the $MgO–2B_2O_3–4wt\%BCB–ywt\%H_3BO_3$ ceramics first increased as the sintering temperature increased up to 900 ℃ and then decreased, demonstrating excellent consistency with varying bulk density. Because there was no secondary phase in the $MgO–2B_2O_3–4wt\%BCB–ywt\%H_3BO_3$ ceramics, the $Q \times f$ was primarily affected by the sintering temperature and H_3BO_3 content, which altered the density and grain size. At a sintering temperature of 850 ℃, the $MgO–2B_2O_3–4wt\%BCB–10wt\%H_3BO_3$ ceramics showed a significant proportion of pores between grains, resulting in a lower $Q \times f$. At 900 ℃, a denser

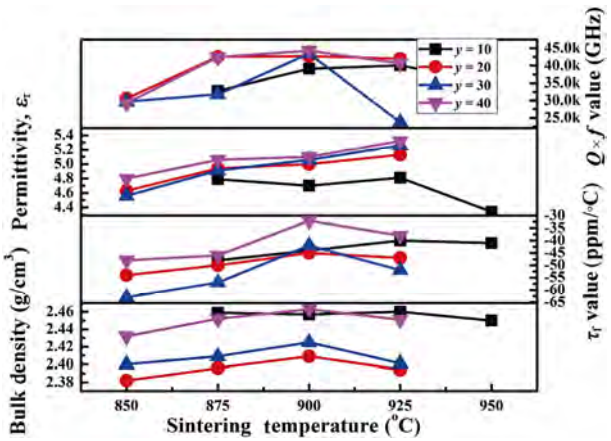

Fig. 6 Bulk density, relative permittivity, $Q \times f$, and τ_f values of the $MgO–2B_2O_3–4wt\%BCB–ywt\%H_3BO_3$ ceramics (y = 10–40) at different sintering temperatures.

microstructure of $MgO–2B_2O_3–4wt\%BCB–40wt\%H_3BO_3$ resulted in a maximum $Q \times f$ of 44,306 GHz, a relative ε_r of 5.1, and τ_f of −32 ppm/℃.

The dielectric properties depend on relative density, crystal structure, and other phase contents [45,46]. The relative ε_r of the $MgO–2B_2O_3–4wt\%BCB–ywt\%H_3BO_3$ ceramics was consistent with the change in bulk density. The maximum ε_r was found to be 4.81 at 10 wt% H_3BO_3. Furthermore, an overall increase in the relative ε_r of the H_3BO_3-containing ceramics was observed when the H_3BO_3 content was increased to 20, 30, and 40 wt%. Hence, the variations in the H_3BO_3 content, sintering temperature, and bulk density influenced ε_r.

Notably, the variations in ρ, ε_r, $Q \times f$, and τ_f values for $MgO–2B_2O_3–4wt\%BCB–ywt\%H_3BO_3$ (y = 10, 20, 30, and 40) were consistent with the changes in the H_3BO_3 content. As mentioned earlier, as the optimal sintering temperature of the $MgO–2B_2O_3–4wt\%BCB–ywt\%H_3BO_3$ ceramics decreased from 925 to 900 ℃, the $Q \times f$, relative ε_r, τ_f, and bulk density increased from 40,076 to 44,306 GHz, from 4.81 to 5.11, from −40 to −32 ppm/℃, and from 2.460 to 2.463 g/cm^3, respectively. The increase in the H_3BO_3 content both lowered the sintering temperature and improved the microwave dielectric properties of the $MgO–2B_2O_3–4wt\%BCB–ywt\%H_3BO_3$ ceramics.

Table 3 tabulates the sintering temperatures and microwave dielectric properties of the $MgO–2B_2O_3–xwt\%BCB–ywt\%H_2BO_3$ ceramics at different BCB and H_3BO_3 contents. When the BCB content was constant, the decrease in the sintering temperature was negligible as the H_3BO_3 content increased. τ_f remained stable at approximately –62 to –32 ppm/℃. When the H_3BO_3 content was constant, the BCB content increased, gradually decreasing the required sintering temperature. The $Q \times f$ increased initially and then decreased at a higher BCB content. In summary, the addition of BCB and H_3BO_3 reduced the sintering temperature and increased the $Q \times f$ of the $MgO–2B_2O_3–xwt\%BCB–ywt\%H_3BO_3$ ceramics. This can be attributed to the growth of the $MgO–2B_2O_3$ grains. The optimal sintering temperature of the produced ceramics reduced to 825 ℃, indicating that it can be used as an alternative material in LTCC devices.

Table 3 Microwave dielectric properties and optimal sintering temperatures of $MgO–2B_2O_3–xwt\%BCB–ywt\%H_3BO_3$ ceramics

Compound	S.T. (℃)	$Q \times f$ (GHz)	ε_r	τ_f (ppm/℃)	Ref.
$MgO–2B_2O_3–2wt\%BCB–10wt\%H_3BO_3$	950 ℃	36,954	4.37	−50	This work
$MgO–2B_2O_3–2wt\%BCB–20wt\%H_3BO_3$	900 ℃	33,591	4.44	−35	
$MgO–2B_2O_3–2wt\%BCB–30wt\%H_3BO_3$	900 ℃	37,251	4.51	−51	
$MgO–2B_2O_3–2wt\%BCB–40wt\%H_3BO_3$	900 ℃	35,981	4.59	−47	
$MgO–2B_2O_3–4wt\%BCB–10wt\%H_3BO_3$	925 ℃	40,076	4.81	−40	
$MgO–2B_2O_3–4wt\%BCB–20wt\%H_3BO_3$	900 ℃	42,708	5.00	−45	
$MgO–2B_2O_3–4wt\%BCB–30wt\%H_3BO_3$	900 ℃	43,425	5.06	−42	
$MgO–2B_2O_3–4wt\%BCB–40wt\%H_3BO_3$	900 ℃	44,306	5.10	−32	
$MgO–2B_2O_3–6wt\%BCB–10wt\%H_3BO_3$	850 ℃	37,917	5.31	−62	
$MgO–2B_2O_3–6wt\%BCB–20wt\%H_3BO_3$	850 ℃	40,465	5.05	−59	
$MgO–2B_2O_3–6wt\%BCB–30wt\%H_3BO_3$	850 ℃	41,477	5.07	−38	
$MgO–2B_2O_3–6wt\%BCB–40wt\%H_3BO_3$	800 ℃	37,718	5.21	−40	
$MgO–2B_2O–8wt\%BCB–10wt\%H_3BO_3$	850 ℃	38,664	5.11	−61	
$MgO–2B_2O_3–8wt\%BCB–20wt\%H_3BO_3$	825 ℃	33,985	5.28	−60	
$MgO–2B_2O_3–8wt\%BCB–30wt\%H_3BO_3$	825 ℃	34,618	5.26	−50	
$MgO–2B_2O_3–8wt\%BCB–40wt\%H_3BO_3$	800 ℃	36,064	5.12	−51	
$(1-x)Zn_3B_2O_6 + xMg_3B_2O_6$	950 ℃	89,600	6.47	48.6	[13]
$Mg_3B_2O_6$ + 55wt%LMZBS	950 ℃	50,000	6.80	−64	[47]
$Mg_3B_2O_6$ + 35%LMBS	950 ℃	21,000	6.50	−49.5	[48]

Note: S.T. means sintering temperature.

4 Conclusions

In summary, MgO–$2B_2O_3$–*x*wt%BCB–*y*wt%H_2BO_3 (*x* = 2, 4, 6, and 8; *y* = 10, 20, 30, and 40) ceramics were prepared using solid-state reaction; the influence of the H_3BO_3 and BCB contents on the bulk density, sintering behaviour, and microwave dielectric properties were systematically investigated. The MgO–$2B_2O_3$–*x*wt%BCB–10wt%H_3BO_3 (*x* = 2, 4, 6, and 8) ceramics consisted of a single-phase MgO–$2B_2O_3$ with the orthorhombic space group *Pbca*. The $Q \times f$ of the MgO–$2B_2O_3$–*x*wt%BCB–10wt%H_3BO_3 (*x* = 2, 4, 6, and 8) ceramics increased initially and then decreased gently as the BCB content increased. The optimal properties of the resulting MgO–$2B_2O_3$–4wt%BCB–10wt%H_3BO_3 ceramic were ρ = 2.409 g/cm^3, $Q \times f$ = 40,076 GHz, ε_r = 5, and τ_f = −45 ppm/℃. In addition, the microwave dielectric properties and sintering temperature of the MgO–$2B_2O_3$–4wt%BCB–*y*wt%H_3BO_3 ceramics (*y* = 10, 20, 30, and 40) improved as the H_3BO_3 content increased at 4 wt% BCB. The resulting MgO–$2B_2O_3$–4wt%BCB–40wt%H_3BO_3 demonstrated excellent microwave dielectric properties, with ε_r, $Q \times f$, and τ_f of 5.1, 44,306 GHz (at 15 GHz), and −32 ppm/℃, respectively. This study presented a novel approach to modify the τ_f of MgO–B_2O_3 ceramics, which is an important parameter that governs the stability and performance of microwave equipment and devices.

Acknowledgements

This work was supported by the National Natural Science Foundation of China (Nos. 61761015 and 12064007), the Natural Science Foundation of Guangxi (Nos. 2018GXNSFFA050001, 2017GXNSFDA198027, and 2017GXNSFFA198011), High Level Innovation Team and Outstanding Scholar Program of Guangxi Institutes.

References

[1] Sebastian MT, Jantunen H. Low loss dielectric materials for LTCC applications: A review. *Int Mater Rev* 2008, **53**: 57–90.

[2] Zhou HF, Liu XB, Chen XL, *et al*. $ZnLi_{2/3}Ti_{4/3}O_4$: A new low loss spinel microwave dielectric ceramic. *J Eur Ceram Soc* 2012, **32**: 261–265.

[3] Zhou D, Guo D, Li WB, *et al*. Novel temperature stable high-ε_r microwave dielectrics in the Bi_2O_3–TiO_2–V_2O_5 system. *J Mater Chem C* 2016, **4**: 5357–5362.

[4] Zhou D, Pang LX, Wang DW, *et al*. Novel water-assisting low firing MoO_3 microwave dielectric ceramics. *J Eur Ceram Soc* 2019, **39**: 2374–2378.

[5] Dou G, Zhou DX, Guo M, *et al*. Low-temperature sintered Zn_2SiO_4–$CaTiO_3$ ceramics with near-zero temperature coefficient of resonant frequency. *J Alloys Compd* 2012, **513**: 466–473.

[6] Wang KG, Zhou HF, Liu XB, *et al*. A lithium aluminium borate composite microwave dielectric ceramic with low permittivity, near-zero shrinkage, and low sintering temperature. *J Eur Ceram Soc* 2019, **39**: 1122–1126.

[7] Hughes H, Iddles DM, Reaney IM. Niobate-based microwave dielectrics suitable for third generation mobile phone base stations. *Appl Phys Lett* 2001, **79**: 2952–2954.

[8] Li YX, Li H, Tang B, *et al*. Microwave dielectric properties of low-fired $Li_2ZnTi_3O_8$–TiO_2 composite ceramics with Li_2WO_4 addition. *J Mater Sci*: *Mater Electron* 2015, **26**: 1181–1185.

[9] Hao SZ, Zhou D, Hussain F, *et al*. Structure, spectral analysis and microwave dielectric properties of novel $x(NaBi)_{0.5}MoO_4$–$(1–x)Bi_{2/3}MoO_4$ (x = 0.2 ~ 0.8) ceramics with low sintering temperatures. *J Eur Ceram Soc* 2020, **40**: 3569–3576.

[10] Bi JX, Xing CF, Yang CH, *et al*. Phase composition, microstructure and microwave dielectric properties of rock salt structured Li_2ZrO_3–MgO ceramics. *J Eur Ceram Soc* 2018, **38**: 3840–3846.

[11] Davis HM, Knight MA. The system magnesium oxide-boric oxide. *J Am Ceram Soc* 1945, **28**: 97–102.

[12] Nishizuka M, Ogawa H, Kan A, *et al*. Synthesis and microwave dielectric properties of MgO–*x*mol%B_2O_3 (*x* = 33 and 25) ceramics in MgO–B_2O_3 system. *Ferroelectrics* 2009, **388**: 101–108.

[13] Peng R, Li YX, Su H, *et al*. Three-phase borate solid solution with low sintering temperature, high-quality factor, and low dielectric constant. *J Am Ceram Soc* 2021, **104**: 3303–3315.

[14] Peng R, Su H, Li YX, *et al*. Microstructure and microwave dielectric properties of Ni doped zinc borate ceramics for LTCC applications. *J Alloys Compd* 2021, **868**: 159006.

[15] Peng R, Su H, An D, *et al*. The sintering and dielectric properties modification of Li_2MgSiO_4 ceramic with Ni^{2+}-ion doping based on calculation and experiment. *J Mater Res Technol* 2020, **9**: 1344–1356.

[16] Fan GC, Zhou HF, Chen XL. Optimized sintering temperature and enhanced microwave dielectric performance of $Mg_2B_2O_5$ ceramic. *J Mater Sci*: *Mater Electron* 2017, **28**: 818–822.

[17] Zhou HF, Tan XH, Liu XB, *et al*. Low permittivity MgO–xB_2O_3–yBaCu(B_2O_5) microwave dielectric ceramics for low temperature co-fired ceramics technology. *J Mater Sci*: *Mater Electron* 2018, **29**: 18486–18492.

[18] Zhou HF, Tan XH, Wang KG, *et al*. Microstructure and sintering behavior of low temperature cofired

$Li_{4/5}Mg_{4/5}Ti_{7/5}O_4$ ceramics containing $BaCu(B_2O_5)$ and TiO_2 and their compatibility with a silver electrode. *RSC Adv* 2017, **7**: 44706–44711.

[19] Guo HH, Zhou D, Du C, *et al*. Temperature stable $Li_2Ti_{0.75}(Mg_{1/3}Nb_{2/3})_{0.25}O_3$-based microwave dielectric ceramics with low sintering temperature and ultra-low dielectric loss for dielectric resonator antenna applications. *J Mater Chem C* 2020, **8**: 4690–4700.

[20] Iddles DM, Bell AJ, Moulson AJ. Relationships between dopants, microstructure and the microwave dielectric properties of ZrO_2–TiO_2–SnO_2 ceramics. *J Mater Sci* 1992, **27**: 6303–6310.

[21] Wu JM, Huang HL. Microwave properties of zinc, barium and lead borosilicate glasses. *J Non-Cryst Solids* 1999, **260**: 116–124.

[22] Tzou WC, Yang CF, Chen YC, *et al*. Improvements in the sintering and microwave properties of $BiNbO_4$ microwave ceramics by V_2O_5 addition. *J Eur Ceram Soc* 2000, **20**: 991–996.

[23] Li EZ, Chen YW, Xiong J, *et al*. Low-temperature firing and microwave dielectric properties of Ba–Nd–Ti with composite doping Li–B–Si and Ba–Zn–B glasses. *J Mater Sci*: *Mater Electron* 2016, **27**: 8428–8432.

[24] Kim MH, Lim JB, Kim JC, *et al*. Synthesis of $BaCu(B_2O_5)$ ceramics and their effect on the sintering temperature and microwave dielectric properties of $Ba(Zn_{1/3}Nb_{2/3})O_3$ ceramics. *J Am Ceram Soc* 2006, **89**: 3124–3128.

[25] Huang CL, Weng MH, Lion CT, *et al*. Low temperature sintering and microwave dielectric properties of $Ba_2Ti_9O_{20}$ ceramics using glass additions. *Mater Res Bull* 2000, **35**: 2445–2456.

[26] Zhou HF, Wang H, Zhou D, *et al*. Effect of ZnO and B_2O_3 on the sintering temperature and microwave dielectric properties of $LiNb_{0.6}Ti_{0.5}O_3$ ceramics. *Mater Chem Phys* 2008, **109**: 510–514.

[27] Li EZ, Niu N, Wang J, *et al*. Effect of Li–B–Si glass on the low temperature sintering behaviors and microwave dielectric properties of the Li-modified ss-phase Li_2O–Nb_2O_5–TiO_2 ceramics. *J Mater Sci*: *Mater Electron* 2015, **26**: 3330–3335.

[28] Zhou D, Pang LX, Wang DW, *et al*. High permittivity and low loss microwave dielectrics suitable for 5G resonators and low temperature co-fired ceramic architecture. *J Mater Chem C* 2017, **5**: 10094–10098.

[29] Pang LX, Zhou D, Qi ZM, *et al*. Structure–property relationships of low sintering temperature scheelite-structured $(1-x)BiVO_4$–$xLaNbO_4$ microwave dielectric ceramics. *J Mater Chem C* 2017, **5**: 2695–2701.

[30] Lu XY, Fang BJ, Zhang S, *et al*. Decreasing sintering temperature for BCZT lead-free ceramics prepared via hydrothermal route. *Funct Mater Lett* 2017, **10**: 1750046.

[31] Huang CL, Wang JJ, Huang CY. Sintering behavior and microwave dielectric properties of nano alpha-alumina. *Mater Lett* 2005, **59**: 3746–3749.

[32] Bafrooei HB, Feizpour M, Sayyadi-Shahraki A, *et al*. High-performance $ZnTiNb_2O_8$ microwave dielectric ceramics produced from $ZnNb_2O_6$–TiO_2 nano powders. *J Alloys Compd* 2020, **834**: 155082.

[33] Liu F, Liu SJ, Cui XJ, *et al*. Ordered domains and microwave properties of sub-micron structured $Ba(Zn_{1/3}Ta_{2/3})O_3$ ceramics obtained by spark plasma sintering. *Materials* 2019, **12**: 638.

[34] Bari M, Taheri-Nassaj E. Taghipour-Armaki H. Role of nano- and micron-sized particles of TiO_2 additive on microwave dielectric properties of $Li_2ZnTi_3O_8$–4wt% TiO_2 ceramics. *J Am Ceram Soc* 2013, **96**: 3737–3741.

[35] Yoon SH, Choi GK, Kim DW, *et al*. Mixture behavior and microwave dielectric properties of $(1-x)CaWO_4$–$xTiO_2$. *J Eur Ceram Soc* 2007, **27**: 3087–3091.

[36] Pan HL, Mao YX, Cheng L, *et al*. New $Li_3Ni_2NbO_6$ microwave dielectric ceramics with the orthorhombic structure for LTCC applications. *J Alloys Compd* 2017, **723**: 667–674.

[37] Zhang P, Hao MM, Mao XR, *et al*. A novel low sintering temperature scheelite-structured $CaBiVMoO_8$ microwave dielectric ceramics. *J Alloys Compd* 2020, **840**: 155187.

[38] Lim JB, Nahm S, Kim HT, *et al*. Effect of B_2O_3 and CuO on the sintering temperature and microwave dielectric properties of the $BaTi_4O_9$ ceramics. *J Electroceramics* 2006, **17**: 393–397.

[39] Navias L, Green FL. Dielectric properties of glasses at ultra-high frequencies and their relation to composition. *J Am Ceram Soc* 1946, **29**: 267–276.

[40] Tang B, Guo X, Yu SQ, *et al*. The shrinking process and microwave dielectric properties of $BaCu(B_2O_5)$-added $0.85BaTi_4O_9$–$0.15BaZn_2Ti_4O_{11}$ ceramics. *Mater Res Bull* 2015, **66**: 163–168.

[41] Ullah B, Lei W, Cao QS, *et al*. Structure and microwave dielectric behavior of A-site-doped $Sr_{(1-1.5x)}Ce_xTiO_3$ ceramics system. *J Am Ceram Soc* 2016, **99**: 3286–3292.

[42] Lan XK, Li J, Zou ZY, *et al*. Lattice structure analysis and optimised microwave dielectric properties of $LiAl_{1-x}(Zn_{0.5}Si_{0.5})_xO_2$ solid solutions. *J Eur Ceram Soc* 2019, **39**: 2360–2364.

[43] Ferreira VM, Baptista JL. Preparation and microwave dielectric properties of pure and doped magnesium titanate ceramics. *Mater Res Bull* 1994, **29**: 1017–1023.

[44] Lei W, Lu WZ, Wang XC, *et al*. Effects of $CaTiO_3$ on microstructures and properties of $(1-x)ZnAl_2O_4$–xMg_2TiO_4 (x=0.21) microwave dielectric ceramics. *J Inorg Mater* 2009, **24**: 957–961.

[45] Zhang P, Zhao YG, Li LX. The correlations among bond ionicity, lattice energy and microwave dielectric properties of $(Nd_{1-x}La_x)NbO_4$ ceramics. *Phys Chem Chem Phys* 2015, **17**: 16692–16698.

[46] Zhao YG, Zhang P. High-Q microwave dielectric ceramics using $Zn_3Nb_{1.88}Ta_{0.12}O_8$ solid solutions. *J Alloys Compd* 2016, **662**: 455–460.

[47] Zhou DX, Sun F, Hu YX, *et al*. Low-temperature sintering and microwave dielectric properties of $Mg_3B_2O_6$–LMZBS

composites. *J Mater Sci*: *Mater Electron* 2012, **23**: 981–989.

[48] Dou G, Guo M, Li YX, *et al*. The effect of LMBS glass on the microwave dielectric properties of the $Mg_3B_2O_6$ for LTCC. *J Mater Sci*: *Mater Electron* 2015, **26**: 4207–4211.